

Graph Signal Entropy for Analyzing Functional Brain Abnormalities of Alzheimer's Disease Patients

Rui Pu, Xiaoying Song^{ID}, Member, IEEE, and Li Chai^{ID}, Senior Member, IEEE

Abstract—A majority of research shows that the brain complexity of Alzheimer's disease (AD) patients is smaller than that of healthy controls (HCs). In this paper, we propose a novel method based on graph signal entropy to investigate the complexity of functional brain networks in AD patients. By using a spectral graph wavelet filter to decompose the subjects' BOLD signal, we generate distinct functional brain networks for each graph frequency band. We then use the multivariate dispersion entropy to examine the abnormal complexity of AD patients across different graph frequency bands. Experimental results reveal that in the low and mid-frequency bands, the brain complexity of AD patients is generally larger than that of HCs, which challenges the conventional understanding that AD is consistently associated with reduced complexity. Moreover, widely reported abnormal brain regions in AD, such as the hippocampus and parahippocampal gyrus, exhibit significant differences only at specific frequency bands, indicating the necessity of frequency-resolved analysis. These findings uncover new characteristics of functional brain networks in AD patients and provide deeper insights into the disease's complex neural mechanisms.

Index Terms—Graph signal entropy, functional brain networks, spectral graph wavelet filter, Alzheimer's disease (AD).

I. INTRODUCTION

ALZHEIMER's disease (AD) is a highly complex neurodegenerative condition [1] and is known to be the most prevalent form of dementia. The prevalence of the disease has been reported to increase exponentially with age growth [2]. In the early stages, AD patients suffer from recent memory loss, which worsens as the disease progresses, as well as a gradual decline in judgement, reasoning and other abilities [3]. In the later stages of the disease, AD patients may completely

Received 25 February 2025; revised 25 August 2025 and 28 September 2025; accepted 8 October 2025. Date of publication 13 October 2025; date of current version 24 October 2025. This work was supported in part by the National Natural Science Foundation of China under Grant 62176192 and Grant 62173259 and in part by Zhejiang Provincial Natural Science Foundation of China under Grant LZ24F030006. (Corresponding author: Xiaoying Song.)

Rui Pu and Xiaoying Song are with the School of Electronic Information, Wuhan University of Science and Technology, Wuhan 430081, China (e-mail: pr@wust.edu.cn; xiaoying811@wust.edu.cn).

Li Chai is with the State Key Laboratory of Industrial Control Technology, College of Control Science and Engineering, Zhejiang University, Hangzhou 310027, China (e-mail: chaili@zju.edu.cn).

This article has supplementary downloadable material available at <https://doi.org/10.1109/TNSRE.2025.3620444>, provided by the authors. Digital Object Identifier 10.1109/TNSRE.2025.3620444

lose the ability to care for themselves and may experience psychological symptoms such as anxiety and depression [4].

Neuroimaging techniques [5] offer valuable tools for investigating the mechanisms of neurological disorders in-depth. One of the most important techniques, functional Magnetic Resonance Imaging (fMRI), estimates brain activity in the form of blood oxygenation level-dependent (BOLD) signals and provides a non-invasive way to study the human brain [6]. The progressive cognitive decline in AD patients is associated with changes in structural and functional connectivity within the brain regions [7]. Viewing the brain as a network of brain regions of interest (ROIs), known as a functional brain network, is an important way of quantifying complex brain interactions. Functional brain networks can be built using a variety of methods, including Pearson correlation, partial correlation, coherence, sparse representation, and other methods that characterize the statistical correlations between BOLD signals on ROIs. If two ROIs show coherent or synchronized dynamics, they are deemed functionally related and perhaps responsive to information interactions [8].

With the help of fMRI, a great deal of findings have been reported on functional brain abnormalities. In particular, AD patients have the most pronounced functional brain abnormalities of any diseases [9], [10]. The notable abnormal brain regions in AD patients include hippocampus, parahippocampal gyrus, inferior temporal gyrus, inferior frontal gyrus, angular gyrus, etc. [11], [12]. There are also researches on entropy measurements of magnetoencephalography (MEG) and electroencephalograph (EEG) data. Almost all investigations led to the same conclusion: AD patients' signals tend to become more predictable as entropy and complexity diminish [13], [14].

These findings not only allow us to understand how the brain processes information during complex cognitive tasks, but also reveal changes in functional brain networks in different disease states. By comparing the properties of the networks in AD patients and HCs and using them as features to identify neurological disorders [15], we can detect signs of AD earlier and thus provide timely interventions for AD patients.

The human brain is a spatio-temporally extended system. Suppose the subject's brain is divided into N brain regions, each with a one-dimensional BOLD time series, which we refer to as the N -channel time series, or the high-dimensional signal on the graph.

In order to investigate the differences between the BOLD signals of AD patients and HCs, as well as the abnormal brain regions, we propose the method of graph signal entropy, which combines spectral graph wavelet transform (SGWT) and multivariate dispersion entropy, with a focus not only on the high-dimensional graph signal but also on its decompositions in the graph frequency bands.

SGWT is an emerging multi-scale decomposition technique of graph signals that is remarkably effective in dealing with complex structured data [16], [17]. Here, we construct distinct functional brain networks for each graph frequency band that are obtained by breaking down the subjects' BOLD signal using a spectral graph wavelet filter. We then apply multivariate dispersion entropy to investigate the abnormal complexity of the AD patients' signal across these various graph frequency bands. Note that previous studies [13], [14], [18], [19] without graph structure considered single-channel time series for each brain region, ignoring the structural information between brain regions. After the spectral graph wavelet filtering of the high-dimensional graph signal, the signals of each band contain not only the temporal information of the brain regions, but also the structural information between brain regions. Based on the calculation of graph signal entropy, we can deeply explore the abnormal brain regions of AD patients and locate the graph frequency bands of the abnormal brain regions.

The proposed method provides a novel and more effective way to understand the functional brain networks of AD patients in the sense that past researches only focused on the temporal features of the BOLD signal, without considering different features in different graph frequency bands. We get the following new findings: 1) We find that the brain entropy of AD patients is not always lower than that of HCs (an existing conclusion that is widely shared). 2) We find that those widely reported abnormal brain regions, such as the hippocampus and parahippocampal gyrus, only show abnormalities at some particular frequency scales.

The rest of the paper is arranged as follows. Section II introduces the related work. Section III presents the details of the proposed method. Section IV introduces the datasets used in this paper and the experimental settings, and then present experimental results. Section V discusses the validity and limitations of the proposed method and explores future research directions. Section VI concludes the paper.

II. RELATED WORK

In this section, we summarise the entropy-based research in AD and the results of existing studies on abnormal brain regions in AD patients.

A. Entropy Study in AD

Information entropy is a central concept in information theory, first proposed by Claude Shannon in 1948 [20], which is used to measure the uncertainty and the amount of information in a system. Consequently, the entropy of time series quantitatively describes the complexity and uncertainty of time series [21].

In the field of neuroscience, various entropy algorithms have been proposed to analyze complex neuroimaging data, particularly EEG and MEG signals. Almost all research support the conclusion that AD patients' signals become more predictable and their entropy and complexity tend to decrease. Fuzzy entropy [18], [19], [22], sample entropy [23], [24], permutation entropy [25], [26], spectral entropy [27] and approximate entropy [28], [29] have all been found to be decreased in AD patients for EEG and MEG signals.

In addition, the application of entropy algorithms to fMRI data is drawing attention and researchers have obtained the similar findings. For example, Wang et al. [13] found a significant reduction in the permutation entropy of functional brain networks in AD patients based on fMRI BOLD signals. Niu et al. [14] found that those brain regions in AD patients with reduced sample entropy were significantly associated with cognitive decline.

B. Graph-Based Analysis for AD

In recent years, graph-based analytical frameworks have emerged as effective tools for characterizing the topological and functional organization of brain networks in AD. Toussaint et al. [30] integrated entropy-based indices with graph-theoretical metrics to examine alterations within the default mode network (DMN) in both normal aging and AD, revealing substantial disruptions in functional connectivity. Their findings demonstrated the capability of graph theory to capture complex inter-regional interactions underlying neurodegenerative processes. Khazaee et al. [31] applied machine learning to resting-state fMRI data using features derived from graph-theoretical measures, achieving high diagnostic accuracy and illustrating the discriminative power of graph-based representations for clinical classification. Faskhodia et al. [32] investigated brain regions implicated in AD pathology and identified significant connectivity changes, emphasizing the contribution of region-specific network disruptions to disease progression. Arpanahi et al. [33] employed longitudinal resting-state fMRI data combined with graph-theoretical modeling to map the evolution of brain network properties across different stages of AD, offering valuable insights into the dynamic reconfiguration of functional networks over time. These studies collectively highlight the significant contributions of graph-based analysis in understanding the functional changes in AD and lay the foundation for our current investigation into the brain network complexity using a novel graph signal entropy method.

C. Investigation of Abnormal Brain Regions in AD

As a neurodegenerative disease primarily characterised by cognitive decline and memory loss, one of the pathological hallmarks of AD is structural and functional changes in certain regions of the brain. Here, we summarise the abnormal brain regions that have been identified in AD patients.

It is now well known that abnormalities in the hippocampus lead to dementia, and significant hippocampal atrophy is the most prominent feature of AD patients [34], [35]. The hippocampus is a core region for memory consolidation

and learning and plays a crucial role in the pathological development of AD. Further studies show that immature neurons in the hippocampus of AD patients have abnormal protein expression, leading to an abnormal increase in neuronal processes [36].

The second predominant region is the parahippocampal gyrus, which is an active component of the limbic system and is responsible for the formation and retrieval of visual memory. Studies have shown that the size of the parahippocampal gyrus is abnormally reduced in AD patients [37], [38], and the disruption of functional connectivity in this region is associated with the functional decline in AD patients [39].

The inferior temporal gyrus, another major abnormal brain region in AD patients, is located below the temporal lobe and is connected to the posterior inferior occipital gyrus, which is critical for the processing of visual information. Voxel morphometry has shown a significant reduction in grey matter volume in the inferior temporal gyrus in AD patients [40]. Probabilistic tractography studies based on diffusion tensor imaging show increased abnormal connectivity between white matter in this region in AD patients [41].

The inferior frontal gyrus, which is responsible for motor control, decision-making, emotion regulation, social cognition, and attentional control, is critical for higher cognitive functions and emotional expression. Activation of the inferior frontal gyrus has been found to be significantly reduced in AD patients, particularly during patterns of sustained attention and distraction [42].

The right angular gyrus, which plays multiple roles in perception, spatial cognition, language comprehension, mathematical analysis, and other functions, has been shown to have significantly lower levels of glucose metabolism during the transition to AD in healthy individuals [43], [44].

The medial frontal cortex is important for maintaining arousal and purposeful behavior. Studies have shown that the decline in cognitive ability, physical functioning, and independence in AD patients is associated with atrophy in this brain region of the brain [45], [46].

The cerebellum, which plays an important role in controlling and coordinating movement, has been shown to atrophy significantly in AD patients as the disease progresses [47].

III. METHOD

In this section, we present the method of graph signal entropy, which can evaluate the entropy characteristics of AD patients at different graph frequency bands. Fig. 1 shows the flowchart of our proposed framework. Firstly, we design a spectral graph wavelet filter to decompose the BOLD signal into wavelet coefficients at multiple graph frequency bands. At each band, different functional brain networks are constructed based on the Pearson correlation between the wavelet coefficients. Then we generate multi-channel signals for brain regions based on the neighborhood information, and calculate the graph signal entropy of brain regions at different bands. Finally, statistical analysis is used to identify abnormal brain regions in AD patients. The details of each step are explained below.

A. Brain Graph

The brain graph can be represented by $G = (V, E, W)$ where $V = \{v_1, v_2, \dots, v_N\}$ represents the set of N ROIs, $E = \{e_{ij} | i, j \in V\}$ is the edge set describing the connections between the ROIs, and $W \in \mathbb{R}^{N \times N}$ is the weighted adjacency matrix obtained by the Pearson correlation between the BOLD signals on brain regions (the most commonly used statistical measure of the relationship between brain regions). If there is no edge between vertices v_i and v_j , or w_{ij} is less than a certain threshold, we set $w_{ij} = 0$.

The Laplacian matrix of G is defined as $L = D - W$, where $D = \text{diag}\{d_i\}$ is the degree matrix and $d_i = \sum_j w_{ij}$. L has semi-positive definite, symmetric properties and can be eigenvalue decomposed as $L = U \Lambda U^T$. $U = \{u_i, i = 1, 2, \dots, N\}$ are the eigenvectors of L , forming an orthonormal basis. $\text{diag}\{\lambda_i\}$ are the eigenvalues of L , and satisfy $\{0 \leq \lambda_1 \leq \lambda_2 \leq \dots \leq \lambda_N\}$.

The eigenvalues λ_i of L can be interpreted as the frequencies of G , and the eigenvectors u_i are the corresponding frequency components on the graph. Small values of λ_i indicate lower frequencies and larger values indicate higher frequencies. Given a graph signal $X : V \rightarrow \mathbb{R}^N$ on G , we can define the component of the graph Fourier transform (GFT) of X at the i th frequency to be

$$\widehat{X}(i) = \langle u_i, X \rangle = \sum_{j=1}^N u_i^T(j) X(j). \quad (1)$$

The corresponding graph Fourier inverse transform is

$$X(j) = \sum_{i=1}^N \widehat{X}(i) u_i(j). \quad (2)$$

B. Design of Spectral Graph Wavelet Filter

The Spectral Graph Wavelet Transform (SGWT) enables multiscale analysis of signals defined on graphs by leveraging the graph Laplacian's eigenstructure. Unlike traditional wavelet transforms that operate on regular grids, SGWT applies localized spectral filters to graph-based signals, enabling simultaneous localization in both the spatial and spectral domains. This approach is particularly suited for brain network analysis, where nodes represent brain regions and edges encode functional connectivity. SGWT captures both global patterns and localized fluctuations in brain activity, making it ideal for analyzing dynamic brain signals, such as those from resting-state fMRI. The following mathematical formulation describes the SGWT operator and its application to brain network signals.

Similar to the classical wavelet transform, the key to the SGWT is the design of the spectral graph wavelet kernel $g(x)$ and the scaling function kernel $h(x)$. Let the wavelet operator to be $T_g = g(L)$ and the scaling function operator to be $T_h = h(L)$.

The wavelet operators on the scale factor t ($t = t_1, t_2, \dots, t_S$) are defined as $T_g^t = g(tL)$.

Then, the spectral graph wavelet at a single vertex v_j can be expressed as

$$\psi_{t,j}(l) = \sum_{i=1}^N g(t_s \lambda_i) u_i^*(j) u_i(l). \quad (3)$$

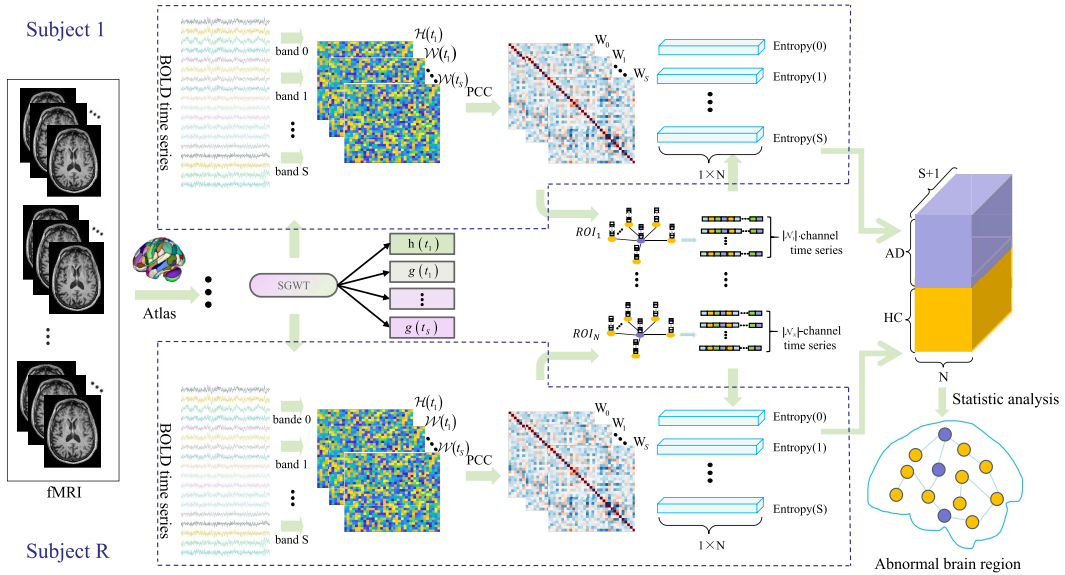


Fig. 1. Flowchart of the proposed graph signal entropy.

The scaling function can be defined as

$$\phi_j(l) = \sum_{i=1}^N h(t_1 \lambda_i) u_i^*(j) u_i(l). \quad (4)$$

Combining the scaling coefficients $\mathcal{H}_X(t_1, j) = \langle \phi_j, X \rangle = \sum_{i=1}^N h(t_1 \lambda_i) \hat{X}(i) u_i(j)$ and the wavelet coefficients $\mathcal{W}_X(t_s, j) = \langle \psi_{t_s, j}, X \rangle = \sum_{i=1}^N g(t_s \lambda_i) \hat{X}(i) u_i(j)$ of X , we obtain the SGWT coefficients of X (frequencies from low to high): $\{\mathcal{H}_X(t_1); \mathcal{W}_X(t_1); \dots; \mathcal{W}_X(t_s)\}$.

To achieve fine scale localisation, $g(x)$ should satisfy $g(0) = 0$ and $\lim_{x \rightarrow \infty} g(x) = 0$, which is consistent with the characteristics of a bandpass filter. The scaling function kernel $h(x)$ should satisfy $h(0) > 0$ and $\lim_{x \rightarrow \infty} h(x) = 0$, which is consistent with the characteristics of a lowpass filter. Here, we utilise the Meyer wavelet [16] to complete the design of the spectral graph wavelet filters, whose wavelet kernel $g(x)$ and scaling function $h(x)$ are defined respectively as

$$g(x) = \begin{cases} \sin\left(\frac{\pi}{2}v\left(\frac{3}{2}|x| - 1\right)\right) & \text{if } \frac{2}{3} \leq x \leq \frac{4}{3} \\ \cos\left(\frac{\pi}{2}v\left(\frac{3}{2}|x| - 1\right)\right) & \text{if } \frac{4}{3} \leq x \leq \frac{8}{3} \\ 0 & \text{otherwise} \end{cases} \quad (5)$$

$$h(x) = \begin{cases} 1 & \text{if } 0 \leq x \leq \frac{2}{3} \\ \cos\left(\frac{\pi}{2}v\left(\frac{3}{2}|x| - 1\right)\right) & \text{if } \frac{2}{3} \leq x \leq \frac{4}{3}, \\ 0 & \text{otherwise} \end{cases} \quad (6)$$

where $v(x) = x^4(35 - 84x + 70x^2 - 20x^3)$.

Let the maximum decomposition scale be S and the scale factors $t_s = \frac{4}{3\lambda_{\max}} \cdot 2^{(S-s)}$, $s = 1, 2, \dots, S$. To construct an

appropriate spectral graph wavelet filter, we need to specify the maximum upper bound of the filter, i.e. the maximum eigenvalue λ_{\max} . We construct the brain graph for each subject and select the largest of the maximum eigenvalues for all subjects as λ_{\max} of the filter.

To more comprehensively explore the potential information embedded in BOLD signals, we apply spectral graph wavelet filters to perform multi-band decomposition of brain network graph signals. Compared with traditional time-frequency analysis methods, spectral graph filtering not only considered temporal variations in the signal but also integrated structural connectivity among brain regions, thereby enabling more sensitive detection of local network dynamics and inter-regional differences [48]. Although BOLD signals are predominantly concentrated in the low-frequency range, they exhibit diverse characteristics in the graph frequency domain. Different frequency bands may reflect distinct levels of brain functional organization. Specifically, low graph-frequency components correspond to global coherence and spatial smoothness of the brain network, whereas high graph-frequency components capture rapid transitions and localized fluctuations, which were potentially associated with enhanced functional activity in specific regions [49]. Therefore, the frequency band differences derived from spectral graph wavelet decomposition may carry meaningful neurophysiological implications.

C. Construction of Multi-Band Functional Brain Networks

Suppose there are R subjects in the study, and their fMRI data are pre-processed to extract the BOLD signal for each subject, denoted as $\chi_r \in \mathbb{R}^{N \times T}$, $r = 1, \dots, R$, where T is the length of the BOLD signal. With the spectral graph wavelet filter constructed above, the BOLD signal of a subject can be decomposed into the SGWT coefficients at $S+1$ different graph frequency bands, including a low frequency band $\mathcal{H}(t_1)$ and S high frequency bands $\mathcal{W}(t_s)$, $s = 1, 2, \dots, S$. Based

Algorithm 1 Construction of the Multi-Band Functional Brain Networks

Data: BOLD signals $\chi \in \mathbb{R}^{N \times T}$ of all subjects, wavelet kernel $g(x)$, scaling function $h(x)$, maximum decomposition scale S .

Result: Functional brain networks at $S + 1$ bands $G_s, s = 0, 1, \dots, S$.

- 1 Determine the maximum eigenvalue λ_{\max} and compute scale factors $t_s = \frac{4}{3\lambda_{\max}} \cdot 2^{(S-s)}, s = 1, 2, \dots, S$;
- 2 **for each subject do**
- 3 Compute weighted adjacency matrix using Pearson correlation of χ : $W \in \mathbb{R}^{N \times N}$;
- 4 Perform eigenvalue decomposition of the Laplacian matrix $L = U \Lambda U^T$;
- 5 Apply graph Fourier transform to χ : $\hat{\chi} = U^T \chi$;
- 6 Decompose the signal χ :
- 7 scale 0: $\mathcal{H}(t_1) = h(t_1 \Lambda) \hat{\chi} U \in \mathbb{R}^{N \times T}$;
- 8 **for each high frequency scale s do**
- 9 $\mathcal{W}(t_s) = g(t_s \Lambda) \hat{\chi} U \in \mathbb{R}^{N \times T}$;
- 10 **end**
- 11 Construct the functional brain networks at the low frequency band G_0 ($W_0 \in \mathbb{R}^{N \times N}$) using Pearson correlation of $\mathcal{H}(t_1)$;
- 12 Construct the functional brain networks at high frequency bands G_s ($W_s \in \mathbb{R}^{N \times N}, s = 1, \dots, S$) using Pearson correlation of $\mathcal{W}(t_s)$.
- 13 **end**

on the Pearson correlation between the corresponding wavelet coefficients at each band, we can construct $S + 1$ functional brain networks $G_s, s = 0, 1, \dots, S$ to reflect the interactions between brain regions at different bands. The pseudo-code is given in Algorithm 1. On the basis of these functional brain networks, we propose graph signal entropy, which will be described in detail in the next section.

D. Proposed of the Graph Signal Entropy

We use the concept of multivariate dispersion entropy [50] to deal with the multi-dimensional graph signals on the functional brain networks. We employ the entropy of the brain regions to quantify the intrinsic uncertainty and statistical features of the time series on the brain regions. Then we investigate the abnormal brain regions of AD patients based on changes in the entropy of the brain regions.

Taking the functional brain networks $G_s, s = 0, 1, \dots, S$ of the subject at a certain frequency band as the underlying structure, we set a threshold τ to binarise the weighted adjacency matrix W_s to eliminate weak connections from the networks. The high-dimensional signals on the networks are the corresponding SGWT coefficients ($\mathcal{H}(t_1)$ for G_0 and $\mathcal{W}(t_s)$ for $G_s, s = 1, \dots, S$), which are uniformly denoted as $Y = [Y_1; Y_2; \dots; Y_N] \in \mathbb{R}^{N \times T}$, with $Y_i \in \mathbb{R}^{1 \times T}, i = 1, 2, \dots, N$ for signals on the i th brain region. Then we can construct the $|\mathcal{N}_i|$ -channel time series for the i th brain region $F = \{Y_j | j \in \mathcal{N}_i\} \in \mathbb{R}^{|\mathcal{N}_i| \times T}$, where \mathcal{N}_i is the neighbourhood set of the i th brain region.

The graph signal entropy of F can be used to measure the complexity of activity in this brain region at the current graph frequency band and the algorithm consists of the following five steps:

1) Based on the Normal Cumulative Distribution Function (NCDF) [21], we normalize F by channels, and finally get \tilde{F} , with \tilde{F}_{ij} in the range $(0, 1)$.

2) By the linear transformation $Z = \text{round}(c \cdot \tilde{F} + 0.5)$, we get the dispersion categorical label Z . Each element of \tilde{F} is mapped into one of the integers from 1 to c , where c is the number of categories.

3) Let m and β denote the embedding dimension and the time delay, respectively. Considering both temporal and spatial information, we construct the following embedding matrices $\Psi(o) \in \mathbb{R}^{K \times m}, o = 1, 2, \dots, T - (m - 1)\beta$.

$$\Psi(o) = \begin{bmatrix} z_{1,o}, z_{1,o+\beta}, z_{1,o+2\beta}, \dots, z_{1,o+(m-1)\beta} \\ z_{2,o}, z_{2,o+\beta}, z_{2,o+2\beta}, \dots, z_{2,o+(m-1)\beta} \\ \vdots \\ z_{K,o}, z_{K,o+\beta}, z_{K,o+2\beta}, \dots, z_{K,o+(m-1)\beta} \end{bmatrix} \quad (7)$$

Following the construction of the $K \times m$ embedding matrix $\Psi(o)$, the matrix is flattened into a single vector of mK elements by concatenating its rows. From this vector, all possible unordered combinations of m elements are extracted. Each combination is then transformed into an ordered pattern by preserving the original relative order of its elements (i.e., their positional indices in the flattened vector). The frequency of each resulting dispersion pattern $\pi_{e_1 e_2 \dots e_m}$ is subsequently computed across all embedding matrices.

4) There are a total of c^m possible dispersion patterns for c categories embedded in m dimensions, denoted as $\pi_{e_1 e_2 \dots e_m}$, with index $e_i \in \{1, 2, \dots, c\}, i = 1, 2, \dots, m$. Each embedding matrix $\Psi(o)$ contains at most $\binom{mK}{m}$ dispersion patterns. Statistics on the dispersion patterns that all embedding matrices may contain allow us to obtain the frequency distribution of each potential dispersion pattern:

$$p(\pi_{e_1 e_2 \dots e_m}) = \frac{N_{\pi_{e_1 e_2 \dots e_m}}}{(T - (m - 1)\beta) \cdot \binom{mK}{m}} \quad (8)$$

where $N_{\pi_{e_1 e_2 \dots e_m}}$ represents the number of occurrences of the pattern $\pi_{e_1 e_2 \dots e_m}$, T is the total length of the time series, m is the embedding dimension, β is the time delay, $\binom{mK}{m}$ represents the number of combinations of m elements from a set of mK elements.

5) Finally, the graph signal entropy of the i th brain region at the graph frequency band s , based on the Shannon entropy theory, can be defined as

$$\mathcal{E}(s + 1, i) = - \sum p(\pi_{e_1 e_2 \dots e_m}) \cdot \ln(p(\pi_{e_1 e_2 \dots e_m})). \quad (9)$$

After the SGWT processing, we obtain $(S + 1)$ functional brain networks for each subject at different graph frequency bands. Based on the proposed graph signal entropy, we can analyze the complexity of the time series on the same brain region at the same graph frequency band in the AD patient group and the HC group, so as to explore the abnormal brain regions in the AD patients; on the other hand, we can also analyze the abnormal extent of the same brain region at

different frequency bands, so as to further locate the abnormal frequency band of the abnormal brain regions in the AD patients. In this way, a more comprehensive study of the abnormal brain regions of AD patients can be carried out.

Algorithm 2 The Proposed Graph Signal Entropy Algorithm

```

Data: SGWT coefficients  $\mathcal{H}(t_1), \mathcal{W}(t_1), \dots, \mathcal{W}(t_S)$ 
Result: Graph signal entropy of  $N$  brain regions at  $S + 1$  graph frequency bands  $\mathcal{E} \in \mathbb{R}^{(S+1) \times N}$ 
1 for each subject do
2   for each frequency scale  $s$  do
3     Construct the functional brain network  $G_s$ ;
4   for each brain region do
5     Construct the  $|\mathcal{N}_i|$ -channel time series  $F \in \mathbb{R}^{|\mathcal{N}_i| \times T}$ ;
6   Normalize  $F$  to  $\hat{F}$ ;
7   Obtain the dispersion categorical label  $Z = \text{round}(c\hat{F} + 0.5)$ ;
8   Construct a series of embedding matrices  $\Psi(o) \in \mathbb{R}^{K \times m}, o = 1, 2, \dots, T - (m - 1)\beta$ ;
9   Calculate the frequency distribution of each potential dispersion pattern  $p(\pi_{\varepsilon_1 \varepsilon_2 \dots \varepsilon_m})$ ;
10  Calculate the graph signal entropy  $\mathcal{E}(s + 1, i)$ .
11  end
12 end
13 end
```

The pseudo-code of the proposed algorithm is given in [Algorithm 2](#).

E. Analysis of Abnormal Brain Regions

At each graph frequency band, we perform the two-sample t-test on the graph signal entropy of all brain regions in the AD patient group and the HC group to screen the abnormal brain regions at the current frequency band with the significance level $p < 0.01$. Comparing the results at different frequency bands, the brain regions with repeated occurrences and significance level $p < 0.05$ are statistically analyzed as the predominantly abnormal brain regions in AD patients.

IV. EXPERIMENTS AND RESULTS

A. Datasets and Preprocessing

The dataset used in this experiment is from the Alzheimer's Disease Neuroimaging Initiative (ADNI) and includes 274 subjects from the ADNI-1, ADNI-GO, and ADNI-2 projects, consisting of 105 AD subjects (mean age 74.18 ± 7.54 years, 55 females and 50 males) and 169 HCs (mean age 75.14 ± 3.38 years, 95 females and 74 males). All images are acquired at multiple sites using a 3.0T Philips scanner according to the ADNI protocol [\[51\]](#). The following fMRI scanning parameters are employed and recorded for analysis: repetition time (TR) = 3000 ms, echo time (TE) = 30 ms, flip angle = 80° , slice thickness = 3.3 mm, matrix size = 64×64 , and $T = 140$ volumes.

In this study, the standardized procedure provided by the CONN toolbox [\[52\]](#) (version 20b, accessed from <https://www.nitrc.org/projects/conn>) is utilized in conjunction with

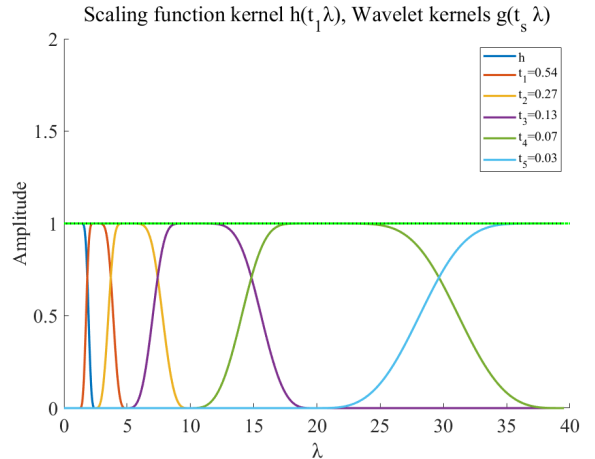


Fig. 2. The spectral graph wavelet filter waveform of the meyer wavelet.

SPM12 [\[53\]](#) (derived from <http://www.fil.ion.ucl.ac.uk/spm/>) to execute a sequential set of preprocessing procedures on the resting-state fMRI data of subjects. The procedures undertaken consist of motion estimation and correction to rectify and remove image distortions, slice time correction to account for variations in scan acquisition times, and outlier detection to detect and eliminate abnormal scan data. We also perform brain tissue segmentation (grey matter, white matter, and cerebrospinal fluid) and normalisation to the Montreal Neurological Institute (MNI) space. To improve image quality, we incorporate spatial smoothing using a Gaussian kernel that is parameterized by a 6 mm full-width half-maximum (FWHM). We perform covariate regression to control for potential effects of age and sex on BOLD signals. Following these steps, we partition the brain of each subject into $N = 132$ ROIs, of which 91 ROIs are identified by the FSL Harvard-Oxford atlas, which can be further divided into left and right hemispheres, as well as 15 subcortical regions (excluding the cerebral cortex, cerebral white matter, and lateral ventricular regions). A further 26 ROIs are derived from the Automated Anatomical Labelling (AAL) atlas, mainly in the cerebellum. The average of the BOLD signals of all voxels within each brain region is taken as the BOLD signal on that brain region, and finally we can obtain the BOLD signal matrix $\chi \in \mathbb{R}^{N \times T}$ of the subject.

B. Experimental Setting

We construct the brain graph for each subject and obtain the corresponding Laplacian matrices. Based on the eigenvalue decomposition of these Laplacian matrices, the maximum upper bound of the spectral graph wavelet filter is set to be $\lambda_{\max} = 39.53$. In this experiment, too large a setting of the frequency band S can over-decompose the low frequency part of the signal, thus causing the low frequency signal to lose its significance, while too small a setting of S can lead to an insufficiently fine capture of the signal bands. So we set $S = 5$, which means that the signal is decomposed into 6 graph frequency bands, and the corresponding scale factors are $t_1 = 0.54$, $t_2 = 0.27$, $t_3 = 0.13$, $t_4 = 0.07$ and $t_5 = 0.03$. The scaling function kernel $h(x)$ and the wavelet kernels $g(x)$ at all frequency bands of the spectral graph wavelet filter are shown in [Fig. 2](#).

TABLE I

BRAIN REGIONS WITH SIGNIFICANT DIFFERENCES ($p < 0.01$) BETWEEN THE AD PATIENT GROUP AND THE HC GROUP AT MULTIPLE GRAPH FREQUENCY BANDS

Frequency band	ROI No.	ROI name	Abbreviation	p	Effect size	Statistical power
Band 1	1	frontal pole right	FP. R	0.0025	0.3812	0.6819
	82	planum polare right	PP. R	0.0041	0.3647	0.6336
	49	frontal medial cortex	MedFC	0.0047	0.3666	0.6393
Band 2	12	inferior frontal gyrus, pars opercularis left	IFG oper. L	0.0040	0.3430	0.5665
	121	cerebellum 9 left	Cereb9. L	0.0059	0.3519	0.5945
Band 3	28	inferior temporal gyrus, anterior division left	aITG. L	0.0014	0.4164	0.7748
	62	parahippocampal gyrus, anterior division right	PaHC. R	0.0070	0.3480	0.5822
	100	hippocampus right	Hippocampus. R	0.0081	0.3404	0.5583
	41	angular gyrus right	AG. R	0.0092	0.3344	0.5395
	29	inferior temporal gyrus, posterior division right	pITG. R	0.0094	0.3373	0.5486

We select the optimal experimental parameters as time delay $\beta = 1$, embedding dimension $m = 2$, and number of categories $c = 4$. This study is an exploratory statistical analysis that aims to evaluate the complexity alterations of functional brain networks in AD across different graph frequency bands. We do not employ supervised classification or predictive models. All graph signal entropy measures are independently computed from each subject's BOLD signals, and we assess group-level differences using two-sample t -tests, statistical power and effect size. Under this analysis framework, we do not require a training-validation split, and there is no risk of information leakage.

C. Specific Abnormal Brain Region Results

To comprehensively evaluate both the statistical significance and the robustness of the observed group differences, we report p -values, effect sizes (Cohen's d), and statistical power (post-hoc analysis) for all comparisons. Specifically, p -values assess the presence of differences, effect sizes quantify their magnitude, and statistical power reflects the sensitivity of the sample to detect such effects. The two-sample t -test results for graph signal entropy across all brain regions in the AD and HC groups are presented in Table I (uncorrected for multiple comparisons). Significant differences were observed in three of the six frequency bands—band 1, band 2, and band 3—whereas the low graph frequency band (band 0) and the high frequency band (band 4) showed no discernible group differences. At the highest frequency band (band 5), all brain regions exhibited significant differences; however, these findings are likely uninformative.

It can be seen that the same brain region behaves differently at different graph frequency bands, and we refer to these abnormal brain regions as specific abnormal brain regions. At band 1, three brain regions show abnormalities in AD patients compared to HCs, which are the right frontal pole (ROI_1), the right planum polare (ROI_82) and the frontal medial cortex (ROI_49). At band 2, there are two abnormal brain regions, the left pars opercularis of inferior frontal gyrus (ROI_12) and cerebellum 9 left (ROI_121). At band 3, many

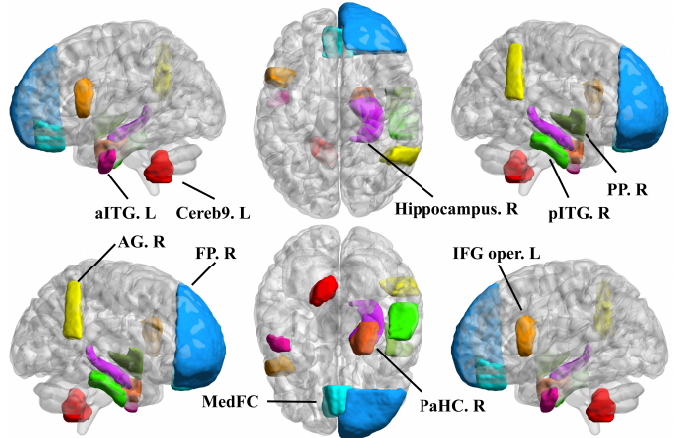


Fig. 3. Locations of specific abnormal brain regions ($p < 0.01$) within the whole brain.

brain regions in AD patients show abnormal activities such as the left anterior division of inferior temporal gyrus (ROI_28), the right anterior division of parahippocampal gyrus (ROI_62), the right hippocampus (ROI_100), the right angular gyrus (ROI_41) and the right posterior division of inferior temporal gyrus (ROI_29).

At the statistical criterion of $p < 0.01$, these specific abnormal brain regions show significant differences only on specific frequency bands, while no significant differences are found on other frequency bands. Fig. 3 shows the locations of these abnormal brain regions within the whole brain. Using graph signal entropy as a novel metric at different frequency bands, the main existing conclusions on abnormal brain regions in AD patients are all reflected in our results. The hippocampus (ROI_100) has been widely reported by existing work [34], [35], [36]. The parahippocampal gyrus (ROI_62) has been widely reported by many work [37], [38], [39]. Existing studies [40], [41] reported the abnormal brain region of inferior temporal gyrus (ROI_28, ROI_29), [42] reported the inferior frontal gyrus (ROI_12), [43], [44] reported the right angular gyrus (ROI_41), [45], [46] reported the frontal medial cortex (ROI_49), and [47] reported the cerebellum (ROI_121).

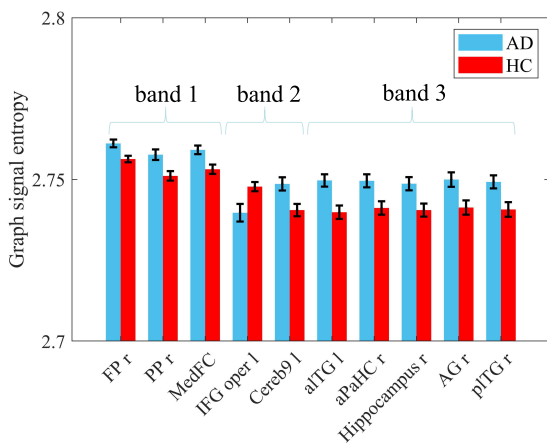


Fig. 4. Graph signal entropy of specific abnormal brain regions ($p < 0.01$).

In addition to the above widely reported brain regions, we discover two new abnormal brain regions that have not been reported, which are the right planum polare (ROI_82) and the right frontal pole (ROI_1). The auditory cortex is part of the auditory cortex and is closely related to speech and auditory processing. The frontal pole plays an important role in specific human behaviours and cognitive abilities. We can reasonably consider these two brain regions as the potential abnormal brain regions in AD patients to help in a more in-depth study of the disease pathology.

D. Entropy Analysis of Specific Abnormal Brain Regions

There have been many studies based on different modalities and different forms of entropy that have shown that the entropy of the AD patient group is smaller than that of the HC group. For example, fMRI-based work [13], [14] revealed that the entropy of the AD patient group is smaller than that of the HC group in all abnormal brain regions. MEG-based work [29] found that the entropy of the AD patient group is smaller. EEG-based work [24], [25], [26], [28] similarly found smaller entropy values for the AD patient group.

For the abnormal brain regions (at different frequency bands) discovered above with significant differences in AD patients, we further analyze the changes in the values of their graph signal entropy, and the results are shown in Fig. 4. It can be seen that the graph signal entropy of the inferior frontal gyrus (ROI_12) in the AD patient group is significantly smaller than that in the HC group at frequency band 2. Except for the inferior frontal gyrus, the graph signal entropy of the AD group is larger than that of the HC group in all other abnormal brain regions. This suggests that the complexity of functional activities in almost all abnormal brain regions (except for the inferior frontal gyrus) is higher in the AD patient group than in the HC group, which is diametrically opposed to the results of existing studies.

This finding suggests that certain brain regions may behave inconsistently during AD pathology when information interactions between brain regions (based on the graph structure) and the changes in the entropy of BOLD signals are fully considered. We venture to speculate that these abnormal brain

TABLE II
GENERIC ABNORMAL BRAIN REGIONS ($p < 0.05$) RECURRING AT MULTIPLE GRAPH FREQUENCY BANDS

Frequency band	ROI No.	ROI name	Abbreviation	p
band 0	82	planum polare right	PP r	0.0351
	29	inferior temporal gyrus, posterior division right	pITG r	0.0377
band 1	82	planum polare right	PP r	0.0041
	12	inferior frontal gyrus, pars opercularis left	IFG oper 1	0.0145
	1	frontal pole right	FP r	0.0025
band 2	12	inferior frontal gyrus, pars opercularis left	IFG oper 1	0.0040
	1	frontal pole right	FP r	0.0345
band 3	82	planum polare right	PP r	0.0115
	29	inferior temporal gyrus, posterior division right	pITG r	0.0094

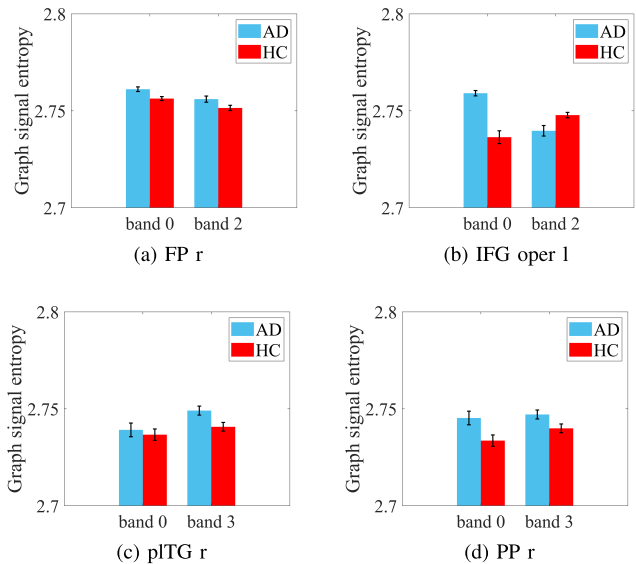


Fig. 5. Graph signal entropy of generic abnormal brain regions ($p < 0.05$) across multiple graph frequency bands.

regions at different graph frequency bands may serve as more advanced features of AD patients.

E. Generic Abnormal Brain Region Results

To explore those abnormal brain regions that show significant differences at multiple graph frequency bands, which we call generic abnormal brain regions, we perform statistics with a looser criterion of $p < 0.05$, and the results are shown in Table II, without correction for multiple comparisons. There are four generic abnormal brain regions, which are the right planum polare (ROI_82), the right posterior division of inferior temporal gyrus (ROI_29), the left pars opercularis of inferior frontal gyrus (ROI_12) and the right frontal pole (ROI_1). We can see that these generic abnormal brain regions derive from specific abnormal brain regions, and that the significant differences they exhibit across multiple frequency bands may be critical to understanding the neuropathological progression of AD patients.

Fig. 5 shows the graph signal entropy analysis of these generic abnormal brain regions over multiple graph frequency bands. It can be seen that the graph signal entropy of the AD patient group is consistently higher than that of the HC group in the right planum polare (ROI_82), the right posterior division of the inferior temporal gyrus (ROI_29) and the right frontal pole (ROI_1) across all observed frequency bands. However, we observe that for the left pars opercularis of the inferior frontal gyrus (ROI_12), the graph signal entropy in the AD patient group is higher than that of the HC group at frequency band 0 and lower than that of the HC group at frequency band 2.

These findings imply that the graph signal entropy properties of the brain in AD patients may have quite different properties at specific frequency bands, which also prompts us to consider the effect of graph frequency bands on the graph signal entropy of brain regions. We can reasonably conclude that different frequency bands may affect the complexity of information processing in brain regions by altering the dynamic interaction patterns and signal strengths of brain networks, which in turn affects the complexity of information processing in brain regions.

F. Analysis of Different Wavelet Types

We employ four types of wavelets—Meyer, Abspline3, Papadakis, and Simoncelli—to construct spectral graph wavelet filters and compare graph signal entropy between AD and HC groups across frequency bands. The filter waveforms are illustrated in Figs. S1–S4, and the corresponding graph signal entropy comparisons appear in Figs. S5–S8. Across all wavelet types, the results remain consistent: AD exhibits higher entropy than HC in low-frequency bands, whereas HC shows higher entropy in high-frequency bands, confirming the robustness of our main conclusion. Among these options, we adopt the Meyer wavelet as the primary filter due to its stronger orthogonality compared with other designs, together with favorable band-pass characteristics, support for multi-scale decomposition, and analytically simple form, which make it particularly well suited for capturing the complexity of graph signals across frequency bands.

V. DISCUSSION

A. Significance of Results

In this paper, we use the largest eigenvalue of the subject's Laplacian matrix as an upper bound to construct the Meyer wavelet kernel function and design the spectral graph wavelet filters to decompose the subject's BOLD signal into multiple graph frequency bands. This process of decomposing the brain signal into multiple frequency bands is essential for understanding the functional activity of the brain and the development of pathological states. It allows for a more refined analysis of brain activity at multiple graph frequency bands, leading to a deeper understanding of the functional brain networks.

To calculate the activity complexity of each brain region at various graph frequency bands, we propose the method of graph signal entropy based on the graph structure. This

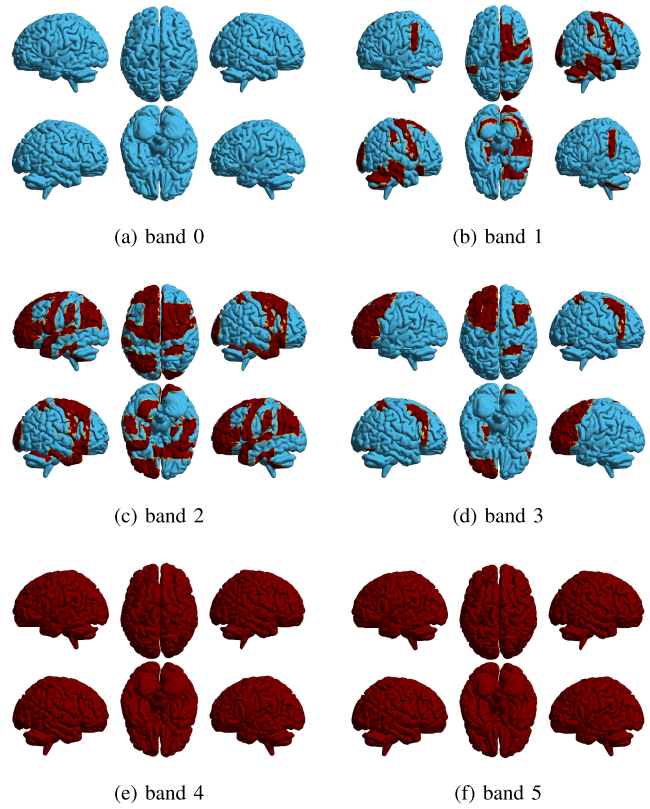


Fig. 6. Comparison of graph signal entropy of the whole brain between the AD patient group and the HC group ($p < 0.01$, brain regions marked in cyan: AD>HC, brain regions marked in red: AD<HC).

algorithm takes into account not only the entropy changes of individual brain regions but also the impact of intricate interactions between brain regions on the entropy of signals. Statistical analysis reveals that the abnormal brain regions of AD patients include the hippocampus, parahippocampal gyrus and other typical brain regions. In addition, we discover two brain regions that have not been reported in previous studies, namely the right frontal pole and the right planum polare. The effective identification of the abnormal brain regions proves the effectiveness of the proposed method in analyzing the functional brain networks of AD patients.

Graph signal entropy is essentially a signal complexity analysis metric that measures the degree of chaos in a signal, with higher complexity indicating greater chaos and lower complexity indicating greater regularity. Analysis of brain signals from multiple graph frequency bands reveals that the entropy of the brain has quite different properties at specific frequency bands. Graph signal entropy quantifies the complexity of energy distribution across graph frequency components. A higher entropy value indicates a more uniform energy distribution and greater disorder in brain activity; A lower entropy suggests more concentrated energy and a more structured, ordered activity pattern [21]. In our findings, AD patients show increased entropy in the low-frequency band, indicating impaired global coordination; and decreased entropy in the high-frequency band, reflecting reduced local processing complexity. As shown in Fig. 6, the entropy of the AD patient group is generally higher than that of the HC group at the low and mid-frequency bands, which contradicts previous studies

and may be due to the fact that researchers did not take into account the spatial interaction information between different brain regions, leading to insufficiently profound conclusions. At the high frequency bands, the entropy of the AD patient group is lower than that of the HC group, which is consistent with the existing findings. This result suggests that conclusions are only rigorous and reliable when entropy changes in AD patients are analyzed at a given graph frequency band.

B. Selection of the Threshold

The selection of the threshold τ for binarizing the weighted adjacency matrix W_s affects the sparsity of the brain network G_s . The larger the value of τ , the sparser the network; conversely, the smaller τ is, the denser the network becomes. The calculation of graph signal entropy relies on the structure of the network, so here we discuss the effect of different thresholds on the experimental results.

Based on the effective empirical range of connection density given by the researchers [54], [55], we additionally select the following different thresholds and analyze their experimental results: 1) $\tau = 0.16$, with a network connection density of about 60%; 2) $\tau = 0.30$, with a network connection density of about 40%; 3) $\tau = 0.39$, with a network connection density of about 30%; 4) $\tau = 0.62$, with a network connection density of about 15%.

In the experiment, we choose $\tau = 0.57$, and the connection density of the network is about 20%, that is, about 20% of the edges in the brain network are connected. The Fig. 6 shows that the entropy of the AD patient group is generally higher than that of the HC group at the low and mid-frequency bands, while the opposite is true at the high frequency bands.

We find that the selection of the threshold affects the results in some brain regions at the low and mid-frequency bands, as shown in Figs. S9-S10. However, in general, the graph signal entropy of most brain regions in AD patients is greater than that of HCs in these graph frequency bands. In particular, when the network becomes dense ($\tau \leq 0.39$), the entropy of all brain regions of AD patients is exactly greater than that of normal subjects. On the other hand, the findings in the high-frequency bands remain constant regardless of threshold changes. We can conclude that the selection of the threshold may affect the results of some brain regions at the low and mid-frequency bands, but has little effect on the overall experimental conclusions.

C. Entropy Analysis in the Time Domain

In addition to analyzing the graph signal entropy of the brain networks in various graph frequency bands, we directly calculate the graph signal entropy of each brain region in the time domain to further validate the effectiveness of the graph signal entropy proposed in this paper. Fig. 7 shows the results of graph signal entropy in the time domain. We observe that the graph signal entropy of the AD patient group is generally lower than that of the HC group in all brain regions, a finding that is consistent with existing findings, demonstrating the validity of our proposed graph signal entropy, and providing



Fig. 7. Comparison of graph signal entropy between the AD patient group and the HC group in the time domain ($p < 0.01$, AD < HC).

strong support for our conclusions that more in-depth and comprehensive findings can be obtained in the graph frequency domain.

D. Network Construction Methods Analysis

In this study, we systematically compare linear (Pearson and partial correlation) and nonlinear (mutual information and kernel trick) approaches for brain network construction to evaluate their effectiveness in characterizing altered brain complexity in AD. The results obtained using mutual information demonstrate substantial instability, as the estimation of marginal and joint probabilities is highly sensitive to discretization parameters. As shown in Figs. S11–S14, the direction of group differences in graph signal entropy varies considerably across different values of the binning parameter θ , with opposite trends emerging across low- and high-frequency bands. By contrast, the kernel trick method (Fig. S15) yields results consistent with the main conclusion of our work—in the low-frequency band, entropy in AD exceeds that of HC, whereas the opposite holds in the high-frequency band. Nevertheless, this approach comes with markedly higher computational costs and reveals significant regional alterations only in limited frequency ranges, thereby showing weaker frequency-specific differentiation. In addition, the partial correlation method (see Figs. S16–S17) reproduces the same low-versus high-frequency pattern, but it does not identify any significant brain regions and presents less pronounced frequency specificity relative to the Pearson correlation method. Collectively, these findings indicate that although nonlinear approaches provide complementary perspectives, their instability, computational burden, and limited interpretability hinder practical application. In contrast, Pearson correlation, with its computational simplicity, robustness, and clear interpretability, offers a reliable framework for capturing the essential linear interactions underlying functional brain networks in AD.

E. Optimal Parameter Selection

An important issue for the proposed graph signal entropy is the selection of appropriate parameters. Here we have three parameters including the time delay β , the embedding dimension m , and the number of categories c . We use the empirical value of $\beta = 1$ for the time delay, because if

$\beta > 1$ some important temporal information can be discarded, leading to aliasing [21], [56].

The embedding dimension m defines the dimensionality of the embedding matrix for characterizing temporal dynamics. $m = 1$ is inadequate since a one-dimensional vector cannot capture temporal variability. Prior studies typically recommend $m = 2$ or 3 [21], [57]. Although $m = 3$ may capture richer dynamics, it introduces higher computational cost and noise. Considering efficiency and stability, we adopt $m = 2$.

The number of categories c controls the discretization granularity of normalized signals. A small c risks coarse representation, whereas a large c increases computational burden and noise sensitivity. The literature suggests a range of 3–8 [56]. We compare results with $c = 3$ –8 under $m = 2$. As shown in Figs. S18–S23 and Table S1, the entropy consistently shows AD > HC in low-frequency bands and HC > AD in high-frequency bands, indicating robustness across parameter settings. Notably, clearer frequency-specific differentiation appears at even c values.

To further identify the optimal configuration, we evaluate $c = 4, 6$, and 8 using multiple statistical indicators (Tables S2–S4), including p -values, Cohen's d , and post-hoc statistical power. Results show that increasing c raises p -values, reduces effect size and power, and increases computational cost. Balancing statistical significance, robustness, and efficiency, we select $m = 2$ and $c = 4$ as the optimal parameters for this study.

F. Limitations and Future Work

There is variability among samples in the ADNI dataset in terms of age, sex, and disease progression, which may affect the stability of the results. Although a standardized preprocessing pipeline is applied, potential confounders such as scanner type and medication use remain difficult to control. To address these limitations, future work conducts large-scale, multi-center analyses with comprehensive sensitivity assessments, while also employing multivariate regression on broader public datasets to rigorously account for confounders and evaluate the generalizability of graph signal entropy across multiple neurodegenerative disorders.

VI. CONCLUSION

In this paper, we propose a novel graph signal entropy to analyze into the complexity of the functional brain networks in AD patients. By decomposing the fMRI BOLD signal and constructing functional brain networks at multiple graph frequency bands, we have revealed an increase in the brain complexity of AD patients at low frequency bands and a decrease at high frequency bands, which is a more comprehensive and in-depth finding that challenges the conventional view that the brain complexity of AD patients is generally smaller than that of HCs. In addition, we have identified two unreported abnormal brain regions, which provide new clues and perspectives for further research on AD. Our analysis provides a new understanding of the abnormal properties of the functional brain networks in AD patients. For future research, it is necessary to introduce the graph frequency band

and entropy analysis of BOLD signals for the diagnosis and treatment of AD patients.

REFERENCES

- [1] M. Seifallahi, A. H. Mehraban, J. E. Galvin, and B. Ghoraani, “Alzheimer’s disease detection using comprehensive analysis of timed up and go test via Kinect V.2 camera and machine learning,” *IEEE Trans. Neural Syst. Rehabil. Eng.*, vol. 30, pp. 1589–1600, 2022.
- [2] Z. Li, H.-I. Suk, D. Shen, and L. Li, “Sparse multi-response tensor regression for Alzheimer’s disease study with multivariate clinical assessments,” *IEEE Trans. Med. Imag.*, vol. 35, no. 8, pp. 1927–1936, Aug. 2016.
- [3] H.-C. Li, P.-Y. Chen, H.-F. Cheng, Y.-M. Kuo, and C.-C. Huang, “In vivo visualization of brain vasculature in Alzheimer’s disease mice by high-frequency micro-Doppler imaging,” *IEEE Trans. Biomed. Eng.*, vol. 66, no. 12, pp. 3393–3401, Dec. 2019.
- [4] Q. Zuo, Y. Shen, N. Zhong, C. L. P. Chen, B. Lei, and S. Wang, “Alzheimer’s disease prediction via brain structural-functional deep fusing network,” *IEEE Trans. Neural Syst. Rehabil. Eng.*, vol. 31, pp. 4601–4612, 2023.
- [5] S. Bollmann and M. Barth, “New acquisition techniques and their prospects for the achievable resolution of fMRI,” *Prog. Neurobiol.*, vol. 207, Dec. 2021, Art. no. 101936.
- [6] Q. Wang et al., “Leveraging brain modularity prior for interpretable representation learning of fMRI,” *IEEE Trans. Biomed. Eng.*, vol. 71, no. 8, pp. 2391–2401, Aug. 2024.
- [7] S. Ribarić, “Detecting early cognitive decline in Alzheimer’s disease with brain synaptic structural and functional evaluation,” *Biomedicines*, vol. 11, no. 2, p. 355, Jan. 2023.
- [8] Z. Fu et al., “Altered static and dynamic functional network connectivity in Alzheimer’s disease and subcortical ischemic vascular disease: Shared and specific brain connectivity abnormalities,” *Human Brain Mapping*, vol. 40, no. 11, pp. 3203–3221, Aug. 2019.
- [9] Y. Gu et al., “Abnormal dynamic functional connectivity in Alzheimer’s disease,” *CNS Neurosci. Therapeutics*, vol. 26, no. 9, pp. 962–971, 2020.
- [10] L. Pini et al., “Age at onset reveals different functional connectivity abnormalities in prodromal Alzheimer’s disease,” *Brain Imag. Behav.*, vol. 14, no. 6, pp. 2594–2605, Dec. 2020.
- [11] A. Fornito, A. Zalesky, and E. Bullmore, *Fundamentals of Brain Network Analysis*. New York, NY, USA: Academic Press, 2016.
- [12] K. J. Friston, “Functional and effective connectivity: A review,” *Brain Connectivity*, vol. 1, no. 1, pp. 13–36, Jan. 2011.
- [13] B. Wang et al., “Decreased complexity in Alzheimer’s disease: Resting-state fMRI evidence of brain entropy mapping,” *Frontiers Aging Neurosci.*, vol. 9, p. 378, Nov. 2017.
- [14] Y. Niu et al., “Dynamic complexity of spontaneous BOLD activity in Alzheimer’s disease and mild cognitive impairment using multiscale entropy analysis,” *Frontiers Neurosci.*, vol. 12, p. 677, Oct. 2018.
- [15] R. Hu et al., “Multi-band brain network analysis for functional neuroimaging biomarker identification,” *IEEE Trans. Med. Imag.*, vol. 40, no. 12, pp. 3843–3855, Dec. 2021.
- [16] Y. Shen, W. Dai, C. Li, J. Zou, and H. Xiong, “Multi-scale graph convolutional network with spectral graph wavelet frame,” *IEEE Trans. Signal Inf. Process. over Netw.*, vol. 7, pp. 595–610, 2021.
- [17] R. Krishna, K. Das, H. K. Meena, and R. B. Pachori, “Spectral graph wavelet transform-based feature representation for automated classification of emotions from EEG signal,” *IEEE Sensors J.*, vol. 23, no. 24, pp. 31229–31236, Dec. 2023.
- [18] Y. Cao et al., “Characterization of complexity in the electroencephalograph activity of Alzheimer’s disease based on fuzzy entropy,” *Chaos, Interdiscipl. J. Nonlinear Sci.*, vol. 25, no. 8, Aug. 2015, Art. no. 083116.
- [19] S. Simons, P. Espino, and D. Abásolo, “Fuzzy entropy analysis of the electroencephalogram in patients with Alzheimer’s disease: Is the method superior to sample entropy?,” *Entropy*, vol. 20, no. 1, p. 21, Jan. 2018.
- [20] A. A. Jaoude, “The paradigm of complex probability and claude Shannon’s information theory,” *Syst. Sci. Control Eng.*, vol. 5, no. 1, pp. 380–425, 2017.
- [21] M. Rostaghi and H. Azami, “Dispersion entropy: A measure for time-series analysis,” *IEEE Signal Process. Lett.*, vol. 23, no. 5, pp. 610–614, May 2016.

- [22] A. S. F. Gaudêncio et al., "Three-dimensional multiscale fuzzy entropy: Validation and application to idiopathic pulmonary fibrosis," *IEEE J. Biomed. Health Informat.*, vol. 25, no. 1, pp. 100–107, Jan. 2021.
- [23] X. Tang, X. Zhang, X. Gao, X. Chen, and P. Zhou, "A novel interpretation of sample entropy in surface electromyographic examination of complex neuromuscular alternations in subacute and chronic stroke," *IEEE Trans. Neural Syst. Rehabil. Eng.*, vol. 26, no. 9, pp. 1878–1888, Sep. 2018.
- [24] D. Abásolo, R. Hornero, P. Espino, D. Álvarez, and J. Poza, "Entropy analysis of the EEG background activity in Alzheimer's disease patients," *Physiological Meas.*, vol. 27, no. 3, pp. 241–253, Mar. 2006.
- [25] B. Deng et al., "Multivariate multi-scale weighted permutation entropy analysis of EEG complexity for Alzheimer's disease," *Cognit. Neurodynamics*, vol. 11, pp. 217–231, Nov. 2017.
- [26] B. Deng et al., "Complexity extraction of electroencephalograms in Alzheimer's disease with weighted-permutation entropy," *Chaos: Interdiscipl. J. Nonlinear Sci.*, vol. 25, no. 4, pp. 487–203, Apr. 2015.
- [27] J. Liu, G. Tan, Y. Sheng, and H. Liu, "Multiscale transfer spectral entropy for quantifying corticomuscular interaction," *IEEE J. Biomed. Health Informat.*, vol. 25, no. 6, pp. 2281–2292, Jun. 2021.
- [28] D. Abásolo, R. Hornero, P. Espino, J. Poza, C. I. Sánchez, and R. de la Rosa, "Analysis of regularity in the EEG background activity of Alzheimer's disease patients with approximate entropy," *Clin. Neurophysiol.*, vol. 116, no. 8, pp. 1826–1834, Aug. 2005.
- [29] R. Hornero, J. Escudero, A. Fernández, J. Poza, and C. Gómez, "Spectral and nonlinear analyses of MEG background activity in patients with Alzheimer's disease," *IEEE Trans. Biomed. Eng.*, vol. 55, no. 6, pp. 1658–1665, Jun. 2008.
- [30] P.-J. Toussaint et al., "Characteristics of the default mode functional connectivity in normal ageing and Alzheimer's disease using resting state fMRI with a combined approach of entropy-based and graph theoretical measurements," *NeuroImage*, vol. 101, pp. 778–786, Nov. 2014.
- [31] A. Khazaee, A. Ebrahizadeh, and A. Babajani-Feremi, "Identifying patients with Alzheimer's disease using resting-state fMRI and graph theory," *Clin. Neurophysiol.*, vol. 126, no. 11, pp. 2132–2141, Nov. 2015.
- [32] M. M. Faskhodi, Z. Einalou, and M. Dadgostar, "Diagnosis of Alzheimer's disease using resting-state fMRI and graph theory," *Technol. Health Care*, vol. 26, no. 6, pp. 921–931, Dec. 2018.
- [33] S. Khodadadi Arpanahi, S. Hamidpour, and K. Ghasvarian Jahromi, "Mapping Alzheimer's disease stages toward its progression: A comprehensive cross-sectional and longitudinal study using resting-state fMRI and graph theory," *Ageing Res. Rev.*, vol. 103, Jan. 2025, Art. no. 102590.
- [34] G. Halliday, "Pathology and hippocampal atrophy in Alzheimer's disease," *Lancet Neurol.*, vol. 16, no. 11, pp. 862–864, Nov. 2017.
- [35] E. McLachlan, J. Bousfield, R. Howard, and S. Reeves, "Reduced parahippocampal volume and psychosis symptoms in Alzheimer's disease," *Int. J. Geriatric Psychiatry*, vol. 33, no. 2, pp. 389–395, Feb. 2018.
- [36] K. Jin, A. L. Peel, and X. O. Mao, "Increased hippocampal neurogenesis in Alzheimer's disease," *Proc. Nat. Acad. Sci. USA*, vol. 101, no. 1, pp. 343–347, 2004.
- [37] A. Shiino, T. Watanabe, K. Maeda, E. Kotani, I. Akiguchi, and M. Matsuda, "Four subgroups of Alzheimer's disease based on patterns of atrophy using VBM and a unique pattern for early onset disease," *NeuroImage*, vol. 33, no. 1, pp. 17–26, Oct. 2006.
- [38] J. P. Kesslak, O. Nalcioglu, and C. W. Cotman, "Quantification of magnetic resonance scans for hippocampal and parahippocampal atrophy in Alzheimer's disease," *Neurology*, vol. 41, no. 1, p. 51, Jan. 1991.
- [39] K. Supekar, V. Menon, D. Rubin, M. Musen, and M. D. Greicius, "Network analysis of intrinsic functional brain connectivity in Alzheimer's disease," *PLoS Comput. Biol.*, vol. 4, no. 6, Jun. 2008, Art. no. e1000100.
- [40] M. Irish, O. Piguet, J. R. Hodges, and M. Hornberger, "Common and unique gray matter correlates of episodic memory dysfunction in frontotemporal dementia and Alzheimer's disease," *Human Brain Mapping*, vol. 35, no. 4, pp. 1422–1435, Apr. 2014.
- [41] G.-W. Kim, K. Park, Y.-H. Kim, and G.-W. Jeong, "Increased hippocampal-inferior temporal gyrus white matter connectivity following donepezil treatment in patients with early Alzheimer's disease: A diffusion tensor probabilistic tractography study," *J. Clin. Med.*, vol. 12, no. 3, p. 967, Jan. 2023.
- [42] Z. Guo et al., "Abnormal changes in functional connectivity between the amygdala and frontal regions are associated with depression in Alzheimer's disease," *Neuroradiology*, vol. 60, pp. 1315–1322, 2018.
- [43] C. Ding, W. Du, Q. Zhang, L. Wang, Y. Han, and J. Jiang, "Coupling relationship between glucose and oxygen metabolisms to differentiate preclinical Alzheimer's disease and normal individuals," *Human Brain Mapping*, vol. 42, no. 15, pp. 5051–5062, Oct. 2021.
- [44] A. Hunt, P. Schöcknecht, M. Henze, U. Seidl, U. Haberkorn, and J. Schröder, "Reduced cerebral glucose metabolism in patients at risk for Alzheimer's disease," *Psychiatry Res., Neuroimaging*, vol. 155, no. 2, pp. 147–154, Jul. 2007.
- [45] E. D. Vidoni, R. A. Honea, and J. M. Burns, "Neural correlates of impaired functional independence in early Alzheimer's disease," *J. Alzheimer's Disease*, vol. 19, no. 2, pp. 517–527, Jan. 2010.
- [46] A. Cajanus et al., "The association between distinct frontal brain volumes and behavioral symptoms in mild cognitive impairment, Alzheimer's disease, and frontotemporal dementia," *Frontiers Neurol.*, vol. 10, p. 1059, Oct. 2019.
- [47] H. M. Gellersen et al., "Cerebellar atrophy in neurodegeneration—A meta-analysis," *J. Neurol., Neurosurgery Psychiatry*, vol. 88, no. 9, pp. 780–788, 2017.
- [48] D. I. Shuman, S. K. Narang, P. Frossard, A. Ortega, and P. Vandergheynst, "The emerging field of signal processing on graphs: Extending high-dimensional data analysis to networks and other irregular domains," *IEEE Signal Process. Mag.*, vol. 30, no. 3, pp. 83–98, May 2013.
- [49] W. Huang, T. A. W. Bolton, J. D. Medaglia, D. S. Bassett, A. Ribeiro, and D. Van De Ville, "A graph signal processing perspective on functional brain imaging," *Proc. IEEE*, vol. 106, no. 5, pp. 868–885, May 2018.
- [50] H. Azami, A. Fernández, and J. Escudero, "Multivariate multiscale dispersion entropy of biomedical times series," *Entropy*, vol. 21, no. 9, p. 913, Sep. 2019.
- [51] C. R. Jack Jr. et al., "The Alzheimer's disease neuroimaging initiative (ADNI): MRI methods," *J. Magn. Reson. Imaging, Off. J. Int. Soc. Magn. Reson. Med.*, vol. 27, no. 4, pp. 685–691, 2008.
- [52] A. Nieto-Castanon, *Handbook of Functional Connectivity Magnetic Resonance Imaging Methods in CONN*. Hilbert Press, 2020.
- [53] J. Ashburner, "SPM: A history," *NeuroImage*, vol. 62, no. 2, pp. 791–800, Aug. 2012.
- [54] Y. Chen et al., "Disrupted brain functional networks in drug-naïve children with attention deficit hyperactivity disorder assessed using graph theory analysis," *Human Brain Mapping*, vol. 40, no. 17, Dec. 2019, Art. no. 4877–4887.
- [55] Q. Wei et al., "Graph theoretical analysis and independent component analysis of diabetic optic neuropathy: A resting-state functional magnetic resonance imaging study," *CNS Neurosci. Therapeutics*, vol. 30, no. 3, p. 14579, Mar. 2024.
- [56] C. Lebreton et al., "PV system failures diagnosis based on multiscale dispersion entropy," *Entropy*, vol. 24, no. 9, p. 1311, Sep. 2022.
- [57] M. Rostaghi, M. R. Ashory, and H. Azami, "Application of dispersion entropy to status characterization of rotary machines," *J. Sound Vib.*, vol. 438, pp. 291–308, Jan. 2019.